How to cite: *Angew. Chem. Int. Ed.* **2024**, *63*, e202411172
doi.org/10.1002/anie.202411172

VIP Interlocked Polymers Very Important Paper

Exploring the Impact of Ring Mobility on the Macroscopic Properties of Doubly Threaded Slide-Ring Gel Networks

*Jongwon Oh[+], Guancen Liu[+], Hojin Kim, Jerald E. Hertzog, Natsumi Nitta, and Stuart J. Rowan**

Abstract: The integration of mechanically interlocked molecules (MIMs) into polymeric materials has led to the development of mechanically interlocked polymers (MIPs). One class of MIPs that have gained attention in recent years are slide-ring gels (SRGs), which are generally accessed by crosslinking rings on a main-chain polyrotaxane. The mobility of the interlocked crosslinking moieties along the polymer backbone imparts enhanced properties onto these networks. An alternative synthetic approach to SRGs is to use a doubly threaded ring as the crosslinking moiety, yielding doubly threaded slide-ring gel networks (dt-SRGs). In this study, a photo-curable ligand-containing thread was used to assemble a series of metal-templated pseudo-[3]rotaxane crosslinkers that allow access to polymer networks that contain doubly threaded interlocked rings. The physicochemical and mechanical properties of these dt-SRGs with varying size of the ring crosslinking moieties were investigated and compared to an entangled gel (EG) prepared by polymerizing the metal complex of the photo-curable ligand-containing thread, and a corresponding covalent gel (CG). Relative to the EG and CG, the dt-SRGs exhibit enhanced swelling behavior, viscoelastic properties, and stress relaxation characteristics. In addition, the macroscopic properties of dt-SRGs could be altered by "locking" ring mobility in the structure through remetalation, highlighting the impact of the mobility of the crosslinks.

Introduction

Mechanically interlocked molecules (MIMs), that feature two or more molecular components bound through mechanical bonds, have received significant attention over several decades owing to their extraordinary topological structures.[1–4] The presence of mechanical bonds in MIMs, exemplified by rotaxanes,[5–12] catenanes,[13–16] and molecular knots,[17–20] can lead to unusual relative component motions, such as elongation, twisting, rotation, and sliding, that impart interesting degrees of conformational freedom. The integration of these mechanical bonds and corresponding component motions into polymer matrices presents new opportunities for achieving structural properties that extend beyond the confines of traditional covalent polymer networks. Consequently, substantial efforts have been devoted to the development of mechanically interlocked polymer architectures (MIPs),[21–25] including polycatenane,[26–30] polyrotaxane,[31–33] [c2]daisy-chain,[34–36] slide-ring gels,[37,38] and catenane crosslinked gels.[39–41]

Among these MIPs, slide-ring gels (SRGs), pioneered by Ito,[31,38,42–50] stand out with their exceptional mechanical properties, primarily driven by ring sliding along linear polymer backbone chains. Such sliding motions within SRGs enable gel networks to be more homogeneous and have efficient stress relaxation, leading to enhanced mechanical properties. Common synthetic approaches to SRGs involve either the covalent crosslinking of macrocycles on a polyrotaxane or the incorporation of a [2]pseudorotaxane crosslinking unit into a polymerization.[38,42–44,51,52] Previous studies have revealed that incorporating only a small amount (<1 mol %) of rotaxane crosslinker into a polymer matrix results in significant changes in swelling, tensile strength,

[*] Dr. J. Oh,[+] Dr. H. Kim, Dr. J. E. Hertzog, Dr. N. Nitta, Prof. S. J. Rowan
Pritzker School of Molecular Engineering
University of Chicago
IL 60637 Chicago (USA)
E-mail: stuartrowan@uchicago.edu

G. Liu,[+] Prof. S. J. Rowan
Department of Chemistry
University of Chicago
IL 60637 Chicago (USA)

Dr. H. Kim
James Franck Institute
University of Chicago
IL 60637 Chicago (USA)

Prof. S. J. Rowan
Chemical Science and Engineering Division and Center for Molecular Engineering
Argonne National Laboratory
IL 60434 Lemont (USA)

[+] These authors contributed equally to this work.

viscoelasticity, and toughness relative to a corresponding covalently crosslinked hydrogel.[51–54] Notably, such changes in macroscopic properties are closely linked to ring mobility. For example, to explore the effect of ring mobility on the mechanical properties of SRGs, Takata and co-workers reported α-cyclodextrin ring-based SRGs systems with varying ring mobility by strategically controlling the number of mechanical bonds, the length of the polymer backbone chains, and/or the sterics of the polymer backbone chains through varying substituents.[55,56] They confirmed that impacting ring mobility results in changes in mechanical properties such as fracture energy, stretchability, and toughness.[55,56]

By far, the majority of the studied MIP structures are singly threaded. A different class of MIP could be accessed by using a single (large) ring that can act as a crosslinking unit by threading two or more polymer chains.[57–60] A route to such materials is the polymerization of a doubly threaded (dt-) pseudo[3]rotaxane (P3R). To access such dt-MIPs, it is essential to rationally design the MIM-based crosslinker and effectively incorporate it into the polymer structure while preventing ring dethreading. Recently, it has been shown that the polymerization of a dt-metallo P3R using step-growth polymerization can yield slide-ring polycatenane -like materials.[57] Here, a photo-curable acrylate-functionalized dt-metallo P3R crosslinker is prepared and copolymerized with oligo(ethyleneglycol methyl ether) acrylate, resulting in the formation of a doubly threaded slide-ring gel network (dt-SRG) (Figure 1a) via a chain-growth process. To better understand the impact of ring mobility on the dt-SRG properties, three different dt-SRGs are prepared (Figures 1a–c) with P3R crosslinkers with varying ring sizes. In addition, two different control polymer networks are also targeted: a corresponding entangled gel (EG) and a covalent gel (CG) (Figures 1d and 1e). Finally, as these dt-SRGs are prepared using metal-ligand templating, it is also possible to "lock" the ring mobility through the addition of metal cations (remetalation, Figure 1f).

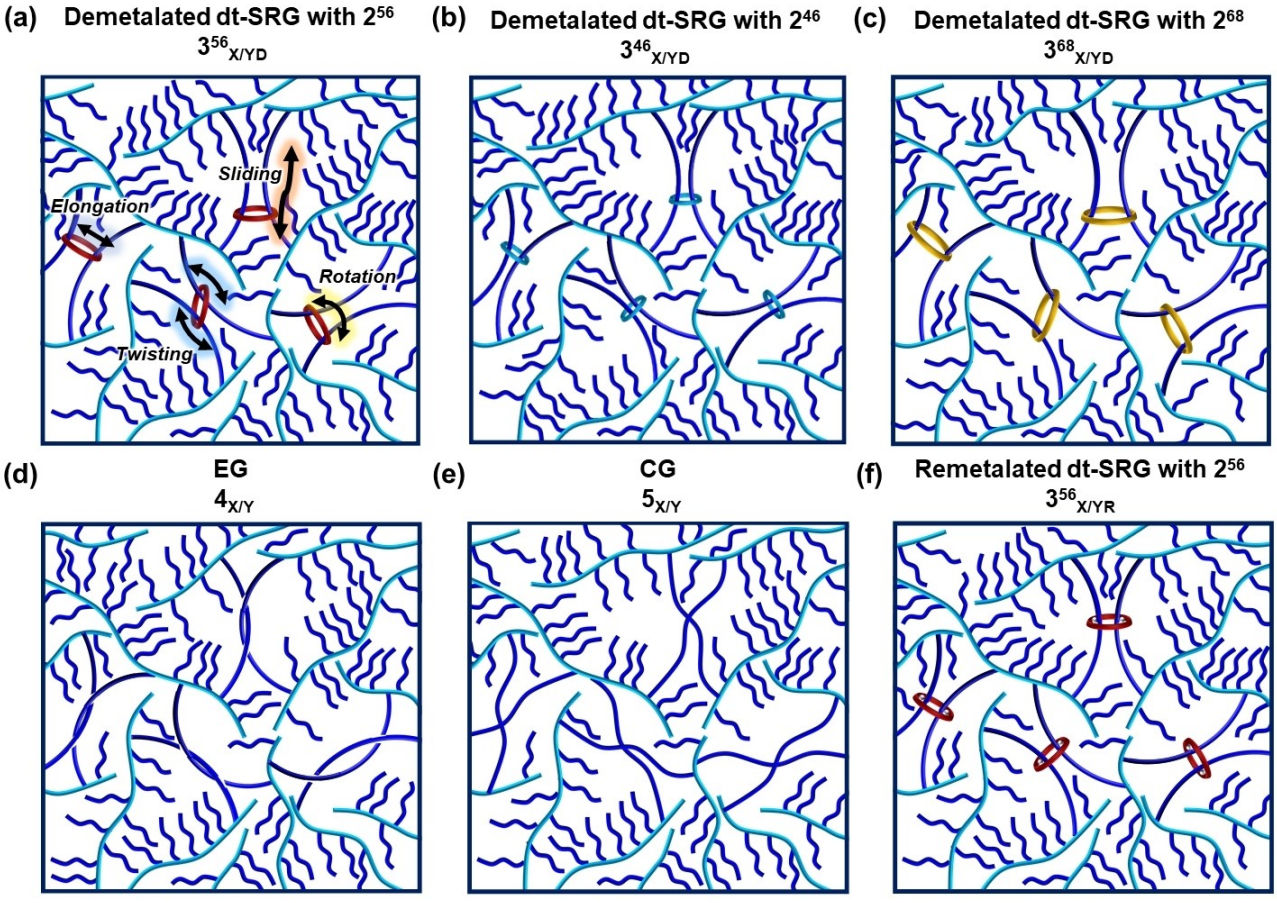

Figure 1. Schematics of doubly threaded slide-ring gel networks (dt-SRGs), entangled gel network (EG), and covalent gel network (CG). (a) Demetalated dt-SRG ($3^{56}_{X/YD}$) with macrocycle 2^{56}, showing selected ring motions (elongation, twisting, rotation, and sliding) attributed to the presence of doubly threaded rings (in red). (b) Demetalated dt-SRG ($3^{46}_{X/YD}$) with smaller rings 2^{46} (light blue) and (c) demetalated dt-SRG ($3^{68}_{X/YD}$) with larger rings 2^{68} (in yellow). Control gel networks: (d) EG ($4_{X/Y}$) and (e) CG ($5_{X/Y}$). (f) Remetalated dt-SRG ($3^{56}_{X/YR}$), exhibiting "locked" ring motions due to the addition of metal cation (in grey). X is the mol% of crosslinker (P3R, 4-arm supramolecular, and covalent crosslinkers) and Y is the mol% of PEG-MA. D and R correspond to a demetalated and remetalated gel, respectively.

Results and Discussion

To access dt-SRGs, doubly threaded P3R crosslinkers were self-assembled utilizing metal-ligand templating with the terdentate 2,6-bis(*N*-alkyl-benzimidazolyl)pyridine (Bip) ligand.[27–29,57–59] The photo-curable thread **1** was synthesized by first reacting a bis-phenolic Bip derivative (*N*,*N*′-Butyl-BipOH) with mono-tosylated nonaethylene glycol, followed by a reaction with acryloyl chloride (Figure 2a and see SM for full synthetic details). The ditopic Bip-containing macrocycle $\mathbf{2^{56}}$ (where the superscript represents the number of atoms comprising the inner circumference of the macrocycles) was accessed by reacting *N*,*N*′-Butyl-BipOH with α,α′-dibromo-*m*-xylene via a Williamson ether synthesis (Figure 2b and see SM for full synthetic details). To allow a study on the impact of ring size in these dt-SRGs, two other macrocycles, $\mathbf{2^{46}}$ and $\mathbf{2^{68}}$, were also synthesized following a similar methodology (Figures 2c and 2d and see SM for full synthetic details). The binding of macrocycles $\mathbf{2^n}$ with Zn(II) was evaluated by UV/Vis titration, confirming that in all cases both Bip ligands in the same macrocycle are not able to bind a single metal cation, and that the addition of two equivalents of Zn(II) results in the formation of the $\mathbf{2^n}$:Zn(II)$_2$ complex (Figure S8).[29,58] Addition of 2 equivalents of zinc di-bis(trifluoromethylsulfonyl)imide (Zn(NTf$_2$)$_2$) to a 2:1 mixture of thread **1** and macrocycle $\mathbf{2^{56}}$ resulted in an instantaneous color change to yellow. The NMR spectra showed the disappearance of the signals around 8.0–8.3 ppm that correspond to unbound pyridyl protons (a and b) of ligand of **1** and $\mathbf{2^{56}}$, while new signals corresponding to these same protons (A and B) in the zinc cation-complex appeared around 8.7–9.1 ppm, consistent with the formation of a doubly threaded P3R crosslinker ($\mathbf{1_2{:}2^{56}{:}Zn(II)_2}$) (Figures 2e and 2f). The P3R crosslinkers with different ring sizes, $\mathbf{1_2{:}2^{46}{:}Zn(II)_2}$ and $\mathbf{1_2{:}2^{68}{:}Zn(II)_2}$, were prepared in a similar manner (Figures 2g and 2h, and see SM for details).

To access dt-SRGs, the photo-initiated copolymerization of $\mathbf{1_2{:}2^{56}{:}Zn(II)_2}$ and poly(ethylene glycol) methyl ether acrylate (PEG-MA, $M_n = 480\ \mathrm{g\,mol^{-1}}$) was conducted with varying compositions of the pre-gel mixture ($\mathbf{1_2{:}2^{56}{:}Zn(II)_2}$ from 1 mol % to 4 mol %, and PEG-MA from 99 mol % to 96 mol %) (Figure 3a, pre-gel solution composition in Table S1). The pre-gel mixture was prepared by dissolving the solid $\mathbf{1_2{:}2^{56}{:}Zn(II)_2}$ and photo-initiator (phenylbis(2,4,6-trimethylbenzoyl)phosphine oxide (BAPO), 0.5 wt %) in the liquid PEG-MA. Subsequent irradiation of the pre-gel solution with long-wavelength ultraviolet light (wavelength: 390–500 nm) initiated free-radical polymerization, generat-

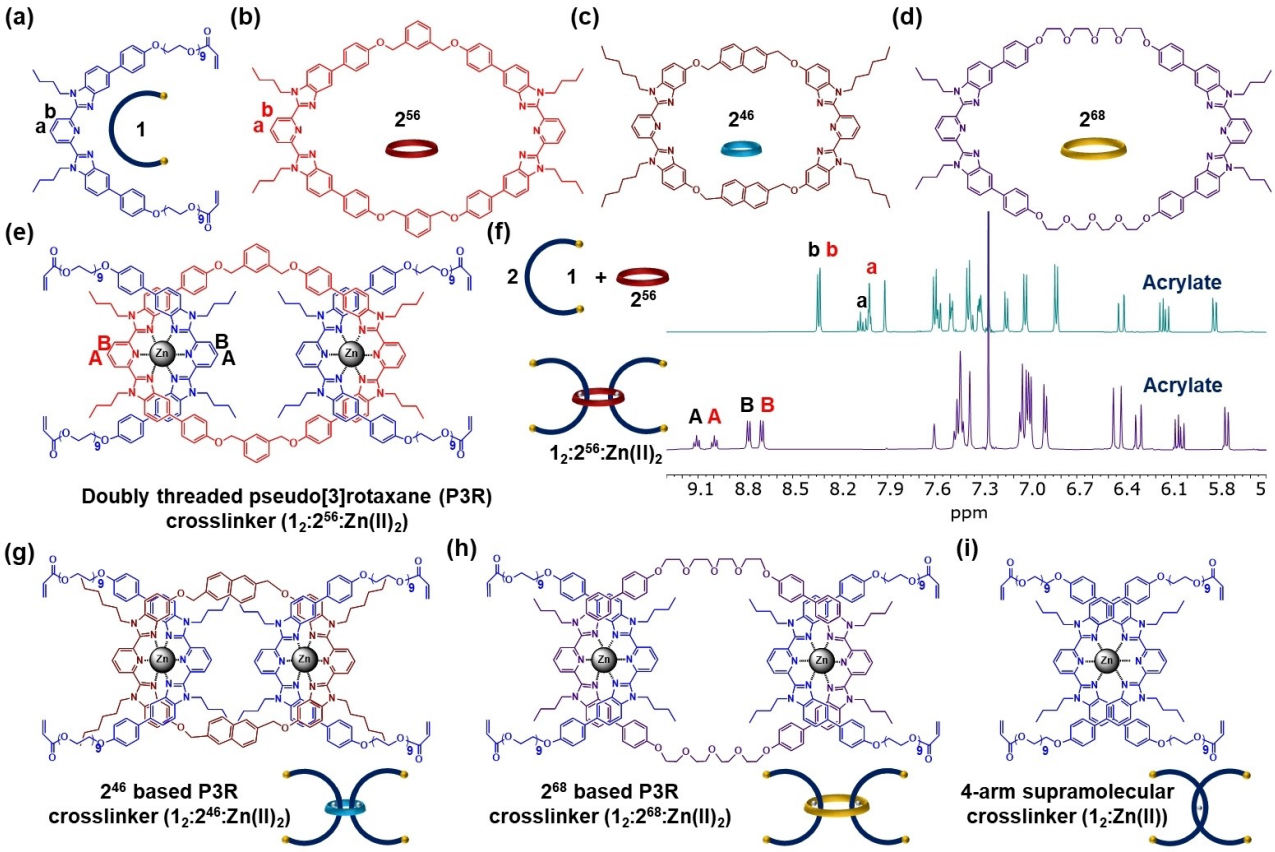

Figure 2. Chemical structures and schematics illustrating (a) photo-curable thread **1**, (b) macrocycle $\mathbf{2^{56}}$, (c) macrocycle $\mathbf{2^{46}}$, and (d) macrocycle $\mathbf{2^{68}}$. (e) Chemical structure of the doubly threaded pseudo[3]rotaxane (P3R) crosslinker $\mathbf{1_2{:}2^{56}{:}Zn(II)_2}$. (f) Partial ^{1}H NMR spectra and schematics of a mixture of $\mathbf{1{:}2^{56}}$ in 2:1 mole ratio (500 MHz, 25 °C, $CDCl_3$) (top) and $\mathbf{1_2{:}2^{56}{:}Zn(II)_2}$ (500 MHz, 25 °C, $CDCl_3$) (bottom). Chemical structures and schematics of (g) $\mathbf{1_2{:}2^{46}{:}Zn(II)_2}$, (h) $\mathbf{1_2{:}2^{68}{:}Zn(II)_2}$, and (i) the 4-arm supramolecular crosslinker $\mathbf{1_2{:}Zn(II)}$.

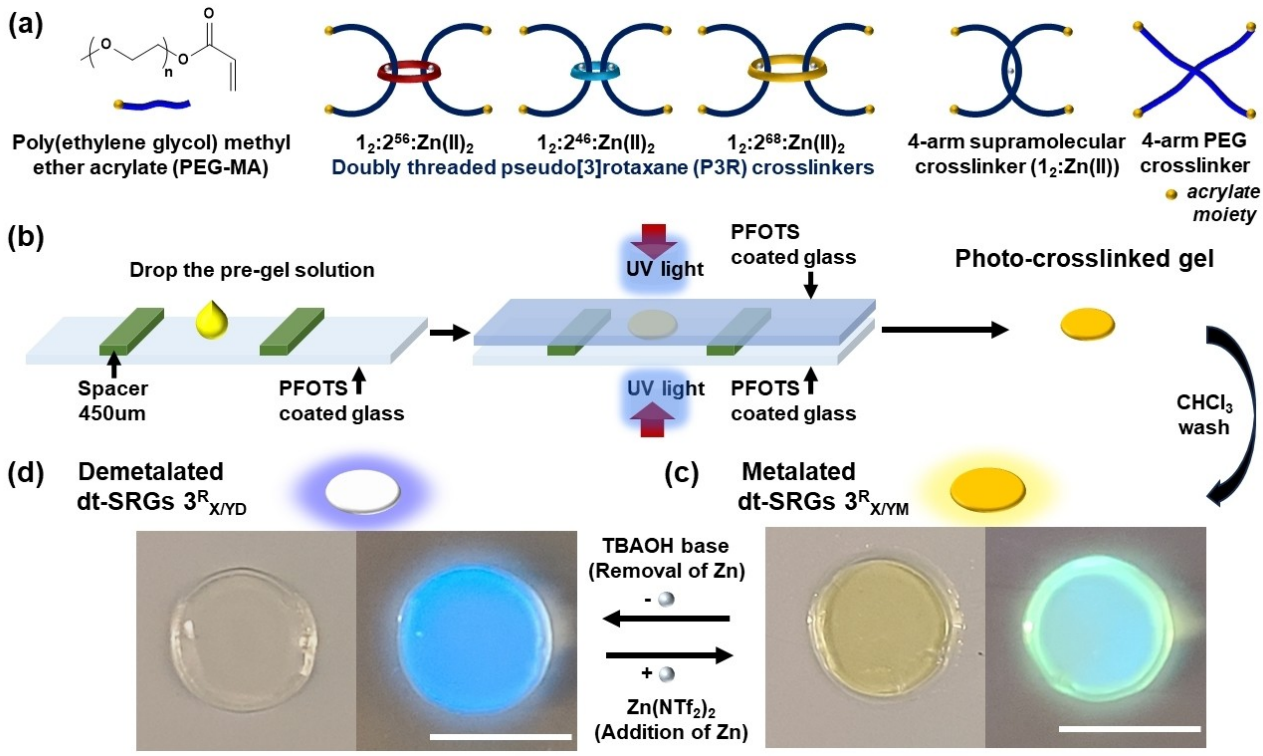

Figure 3. Fabrication of dt-SRGs, EG, and CG. (a) Schematic representations illustrating the pre-gel components used in this study, poly(ethylene glycol) methyl ether acrylate (PEG-MA, $M_n = 480$ gmol^{-1}), the three pseudo[3]rotaxane (P3Rs: $\mathbf{1_2:2^{56}:Zn(II)_2}$, $\mathbf{1_2:2^{46}:Zn(II)_2}$ and $\mathbf{1_2:2^{68}:Zn(II)_2}$) crosslinkers, the 4-arm supramolecular ($\mathbf{1_2:Zn(II)_2}$) crosslinker, and the covalent 4-arm PEG crosslinker. (b) Schematic showing the fabrication process for dt-SRGs, EG, and CG via a photo-crosslinking. Pre-gel solutions were prepared by mixing PEG-MA with the appropriate crosslinker, and the photo-initiator (phenylbis(2,4,6-trimethylbenzoyl)phosphine oxide (BAPO), 0.5 wt%), followed by UV light exposure to induce polymerization into crosslinked gel networks. The residual monomer and initiator were removed by chloroform washing. The type of gel network was determined by the choice of crosslinker (P3R for dt-SRGs, 4-arm supramolecular crosslinker for EGs, and 4-arm PEG crosslinker for CGs). (c) The metalated dt-SRGs $\mathbf{3^R_{X/YM}}$ can be converted to (d) the demetalated dt-SRGs $\mathbf{3^R_{X/YD}}$, via demetalation upon base treatment with TBAOH. The demetalation process occurs with color changes (left) and fluorescence changes (right, excitation by 365 nm UV). (Note: Superscript R represents ring size of 2^R within dt-SRG, subscripts X represents mol% of P3R crosslinker, and Y represents mol% of PEGMA, Y = 100-X). EGs were similarly produced through the similar procedure, including demetalation with TBAOH. Scale bar is 1 cm.

ing the crosslinked network (Figure 3b and see SM for details). Following the removal of the uncrosslinked fraction via chloroform washing, the metalated dt-SRGs $\mathbf{3^{56}_{X/YM}}$ were obtained, where the superscript 56 represents the ring size of $\mathbf{2^{56}}$ within dt-SRG, the subscripts X represents the mol% of P3R crosslinker, Y represents the mol% of PEGMA (Y = 100-X), and M corresponds to the metalated gel. These gel networks had a light yellow-green color and exhibited yellow fluorescence (under 365 nm UV light) attributed to the Bip/Zn(II) complex within the P3R structure (Figures 3c and S17). Subsequently, base treatment with tetrabutylammonium hydroxide (TBAOH) resulted in demetalation of the gel. Iterative washing steps with chloroform and methanol were then employed to effectively extract the soluble fractions and metal salts. The resulting demetalated dt-SRGs, denoted as $\mathbf{3^{56}_{X/YD}}$ where subscript D corresponds to the demetalated gel, exhibited a blue fluorescence characteristic of the free ligand and were characterized by UV/Vis, FT-IR and fluorescence spectroscopy (Figures 3d, S17, and S18). The gel fractions (wt%) of $\mathbf{3^{56}_{X/YD}}$ were evaluated by comparing the weight of the dried gel after photocrosslinking to the weight after demetalation, based on Equation S1 (see SM for details). As the relative amount of tetrafunctional $\mathbf{1_2:2^{56}:Zn(II)_2}$ in the pre-gel solution increased from 1 mol% to 3 mol%, the gel fraction of $\mathbf{3^{56}_{X/YD}}$ increased from 79% to 86% (Figure S21). $\mathbf{3^{56}_{4/96D}}$ exhibited a similar gel fraction to that of $\mathbf{3^{56}_{3/97D}}$.

To confirm the degree of remaining macrocycle in demetalated dt-SRGs $\mathbf{3^{56}_{X/YD}}$, the ring content was determined by analyzing the soluble fractions extracted from both the chloroform washing (soluble fraction of the metalated gel) and the demetalation step (soluble fraction of the demetalated gel). The amount of macrocycles in each soluble fraction was quantified by comparing the macrocycle signal to a reference thymol signal via ^{1}H NMR spectroscopy, and the ring amount was determined using Equations S2–S4 (see SM for details). In all cases, only a small amount of macrocycle $\mathbf{2^{56}}$ was detected in the wash, and the data shows that all the demetalated dt-SRGs $\mathbf{3^{56}_{X/YD}}$ have a high ring content (>97% of the macrocycle added to the reaction, Figure S21), indicating that almost all of the macrocycles from $\mathbf{1_2:2^{56}:Zn(II)_2}$ were incorporated into the

gel networks. Even after 10 days of exposure to chloroform at 50 °C, dt-SRGs retained their ring content without additional dethreading, demonstrating the stability of the gel networks (Figure S22). This ring retention during demetalation and at elevated temperatures is consistent with the formation of an interlocked network.

To better probe the role of the ring crosslinking moieties in these dt-SRGs, two control gel networks were prepared: an entangled gel (EG) and a covalent gel (CG). The EG was synthesized by copolymerization of the 4-arm supramolecular crosslinker (**1_2:Zn(II)**) without a macrocycle, which was prepared via self-assembly of two threads (**1**) with Zn(II) (Figure 2i and see SM for details). The EG **$4_{3/97}$** (Figure 1d) was prepared through the copolymerization of 97 mol % PEG-MA with 3 mol % of **1_2:Zn(II)**, followed by a subsequent demetalation step (see SM for details). The CG **$5_{3/97}$** (Figure 1e) was fabricated by copolymerizing 97 mol % of PEG-MA with 3 mol % of a 4-arm acrylate end-capped PEG-crosslinker (MW = 2000 gmol^{-1}) (see SM for details). Both these control gels had a similar gel fraction to **$3^{56}_{3/97}$** (Figure S23).

The thermal properties of demetalated dt-SRGs **$3^{56}_{X/YD}$** (X = 1–4 mol % of P3R and Y = 100−X mol % of PEG-MA) films, as well as the two controls **$4_{3/97}$** and **$5_{3/97}$**, were characterized using Differential Scanning Calorimetry (DSC). The covalent gel **$5_{3/97}$** exhibits a glass transition temperature (T_g) ca. −63 °C, a cold crystallization temperature (T_{cc}) ca. −41 °C, and melting temperature (T_m) around 0 °C. All the interlocked (**$3^{56}_{X/YD}$**) and entangled (**$4_{3/97}$**) gels exhibit the same three transitions. Both T_g and T_{cc} of **$3^{56}_{X/YD}$** increased as the P3R crosslinker concentration increased from 1 mol % (**$3^{56}_{3/97D}$**) to 3 mol % (**$3^{56}_{3/97D}$**), while dt-SRG **$3^{56}_{4/96D}$** exhibited similar T_g and T_{cc} values to dt-SRG **$3^{56}_{3/97D}$** (Figure S24 and Table S3). Overall, the DSC data showed that the incorporation of macrocycle **2^{56}** does result in a slight inhibition in the amount of cold crystallization and therefore a reduction in the amount of crystallinity of the PEG side chains (Figure S24 and Table S3).

To investigate the physicochemical properties of dt-SRG **$3^{56}_{3/97}$**, the swelling ability was measured in various solvents. Specifically, high-boiling-point solvents such as dimethylformamide (DMF), *N*-methyl pyrrolidone (NMP), propylene carbonate (PC), and dimethyl sulfoxide (DMSO) were utilized for the swelling measurements to minimize evaporation during subsequent mechanical properties testing. The swelling ability of **$3^{56}_{3/97D}$** in the different solvents is shown in Figure 4a, and the weight swelling ratio (wt %) was determined using Equation S5 (see SM for details). As shown in Figure 4b, dt-SRG **$3^{56}_{3/97D}$** exhibits the highest swelling in PC, approximately 730 %, attributed to favorable solvent-polymer interactions, while the swelling of the films in DMSO is much lower, approximately 220 %. The swelling characteristics of dt-SRG could be reversibly tuned through remetalation and demetalation (Figure 4c). Remetalation, which was achieved by the addition of Zn(II) while monitoring UV/Vis and fluorescence spectra to obtain optimal binding, results in a reduced swelling ratio of dt-SRG **$3^{56}_{3/97R}$**, approximately 580 % in PC. Presumably, the addition of Zn(II) induces the "locking" of the ring mobility by re-formation of the Bip/Zn(II) complex (as determined by UV/Fluorescence data, Figure S25) that at least in part results in reduced swelling behavior.

The swelling behavior of the control gels, **$4_{3/97}$** and **$5_{3/97}$**, were also evaluated (Figure 5a). Relative to dt-SRG **$3^{56}_{3/97}$**, the CG **$5_{3/97}$** exhibits a significant reduction in swelling ability (< 400 %), which is consistent with the mobility of the ring allowing greater swelling in the dt-SRGs, as has been observed in other SRG architectures.[31,37,52] The EG **$4_{3/97}$** exhibits swelling abilities in between these two gels and, like the dt-SRG **$3^{56}_{3/97}$**, shows a reduced degree of swelling for the remetalated gel relative to the demetalated gel.

To further probe the effect of the ring crosslinking moieties on the gel networks, the mechanical properties of the fully swollen gels (dt-SRG **$3^{56}_{3/97}$**, EG **$4_{3/97}$**, and CG **$5_{3/97}$**) in PC were examined using dynamic mechanical analysis. The viscoelastic properties of these gels were initially evaluated by measuring the elastic modulus under compressive axial forces. With a small amplitude strain ($\gamma = 1$ %) in the linear viscoelastic regime, storage (E') and loss (E'') moduli were measured using a frequency sweep (Figures 5b and S26). Interestingly, their plateau storage modulus ($E'_{plateau}$) at angular frequency $\omega < 1$ rad/s systematically decreases as there are more possible motions of the crosslinking moieties: $E'_{plateau} = 550$ kPa for **$5_{3/97}$**, $E'_{plateau} = 350$ kPa for **$4_{3/97}$**, and $E'_{plateau} = 150$ kPa for **$3^{56}_{3/97D}$**. Of course, it should be noted that mechanical properties of the gels also correspond their degree of swelling, with the more swollen gels being softer.

Interestingly, dt-SRG **$3^{56}_{3/97D}$** exhibits a distinct "peak" in the loss factor *tan* $\delta = E''/E'$ at 200 rad/s, that is not observed in the CG **$5_{3/97}$**, indicating an additional relaxation process presumably on account of ring mobility. This is further supported by the fact that locking the ring mobility in dt-SRG **$3^{56}_{3/97}$** by the addition of Zn(II) leads to the remetalated dt-SRG **$3^{56}_{3/97R}$** that exhibit mechanical properties similar to those of the CG **$5_{3/97}$**, with an increase in elastic modulus ($E'_{plateau} = 550$ kPa) and the disappearance of the characteristic *tan* δ peak. It is worthy of note that EG **$4_{3/97}$** also exhibits a loss factor peak but at lower frequencies (50 rad/s). Furthermore, the intensity of the *tan* δ peak indicates that **$3^{56}_{3/97D}$**, **$4_{3/97}$**, and **$5_{3/97}$** exhibit varying degrees of energy dissipation, with **$3^{56}_{3/97D}$** exhibiting the largest *tan* δ, suggesting it is the most dissipative gel network, presumably on account of the ring mobility.

To further investigate the relaxation properties at longer timescales and the relationship between gel mechanics and the nature of the crosslinking, macroscopic stress relaxation experiments were carried out under axial deformation (step strain $\gamma = 4$ %) for dt-SRG **$3^{56}_{3/97D}$**, EG **$4_{3/97}$**, and CG **$5_{3/97}$**. The relaxation modulus $E(t)$ was monitored over time t for **$3^{56}_{3/97D}$**, **$4_{3/97}$**, and **$5_{3/97}$** (Figure S27). Figure 5d illustrates representative stress relaxation curves of modulus $E(t)$ normalized by zero-time modulus E_0. Notably, the three different gel networks exhibit dramatically distinct relaxation behaviors depending on the characteristic of their crosslinks. **$3^{56}_{3/97D}$** exhibits significant relaxation, similar to typical behaviors observed in transient gels or dynamic covalent networks.[61–64] The ring mobility of dt-slide ring

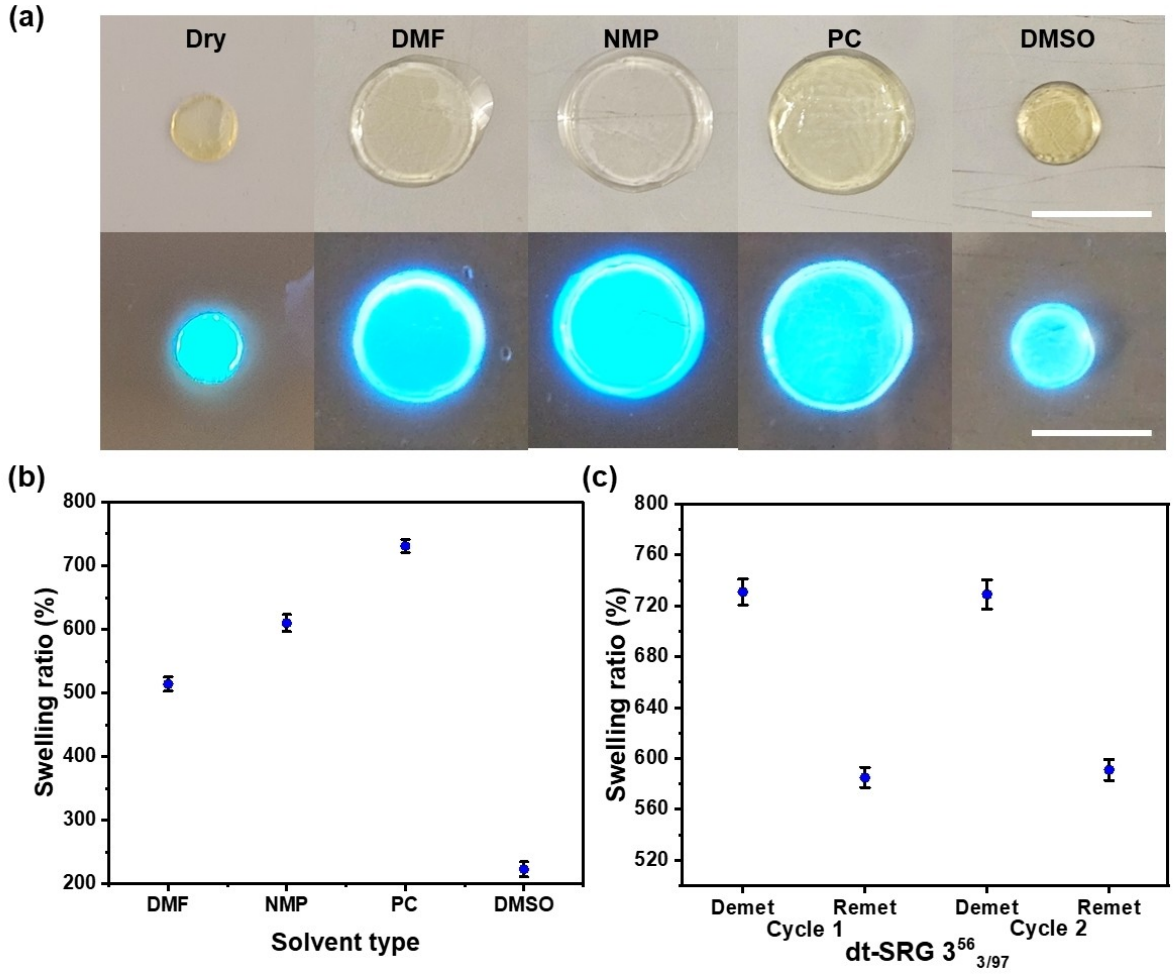

Figure 4. Swelling behaviors of dt-SRG $\mathbf{3}^{56}{}_{3/97}$. (a) Optical (top) and fluorescence (bottom, λ_{ex}: 365 nm) images of demetalated dt-SRG $\mathbf{3}^{56}{}_{3/97D}$ upon exposure to various solvents. (b) Swelling ratios of demetalated dt-SRG $\mathbf{3}^{56}{}_{3/97D}$ when exposed to dimethylformamide (DMF), *N*-methylpyrrolidone (NMP), propylene carbonate (PC), and dimethylsulfoxide (DMSO). (C) Swelling ratios of dt-SRG $\mathbf{3}^{56}{}_{3/97}$ in PC upon remetalation and demetalation. Scale bar is 1 cm.

crosslinks appears to enable the deformed network strands to effectively rearrange, and relax the stress. Thus, dt-SRG $\mathbf{3}^{56}{}_{3/97D}$ exhibits faster relaxation behavior relative to the corresponding covalent gel networks, $\mathbf{5}_{3/97}$. The entangled gel $\mathbf{4}_{3/97}$ exhibits an intermediate relaxation behavior, presumably on account of ability to rearrange the entangled crosslinks. To estimate the relaxation timescale τ, the traditional stretched exponential model $E(t)/E_0 = \boldsymbol{exp}\left(-(t/\tau)^{\beta}\right)$ was employed to fit the stress relaxation curves, with the exponent β being a fitting parameter. While the EG $\mathbf{4}_{3/97}$ and CG $\mathbf{5}_{3/97}$ could both be fitted using this model, the dt-SRG $\mathbf{3}^{56}{}_{3/97D}$ exhibits multiple apparent relaxation behaviors that could not be captured by the stretched exponential with a single relaxation timescale. Instead, the Maxwell-Wiechert model is utilized to account for the multiple relaxation timescales: $E(t)/E_0 = \sum_n E_n \boldsymbol{exp}(-t/\tau_n)$ with the number of elements in parallel $n = 2$. Incorporation of two relaxation timescales results in a good agreement between the experimental data and fitting (Figure 6d, red), with the early-stage relaxation time $\tau_1 = 95$ s and the late-stage relaxation time $\tau_2 = 2400$ s. For comparison, the relaxation time τ for $\mathbf{4}_{3/97}$ was estimated as $\tau = 4000$ s. Notably, the stress relaxation behavior of the dt-SRG $\mathbf{3}^{56}{}_{3/97}$ could be dramatically reduced by locking the ring mobility through the addition of Zn(II) as the remetalated dt-SRG $\mathbf{3}^{56}{}_{3/97R}$ exhibits a much slower stress relaxation behavior, akin to the CG $\mathbf{5}_{3/97}$.

The above data suggest that the presence of the dt-slide ring crosslink has a significant effect on the thermomechanical properties of the gels on account of its mobility. If this is indeed the case, it is reasonable to expect that the ring size in these SRG networks, which should influence the ring mobility, will affect the material's mechanical properties. To investigate the effect of ring size on the dt-SRGs, the dt-SRG $\mathbf{3}^{56}{}_{3/97}$ with a 56-atom ring ($\mathbf{2}_{56}$) was compared to two different dt-SRGs: (1) $\mathbf{3}^{46}{}_{3/97}$ with a smaller a 46-atom ring $\mathbf{2}_{46}$ and (2) $\mathbf{3}^{68}{}_{3/97}$ with a larger 68-atom ring $\mathbf{2}_{68}$ (Figures 1a–c). The dt-SRGs $\mathbf{3}^{46}{}_{3/97}$ and $\mathbf{3}^{68}{}_{3/97}$ were prepared similarly to $\mathbf{3}^{56}{}_{3/97}$, utilizing the P3R crosslinkers $\mathbf{1}_2{:}\mathbf{2}^{46}{:}\mathbf{Zn(II)}_2$ (for $\mathbf{3}^{46}{}_{3/97}$) and $\mathbf{1}_2{:}\mathbf{2}^{68}{:}\mathbf{Zn(II)}_2$ (for $\mathbf{3}^{68}{}_{3/97}$) (See SM for details). All three

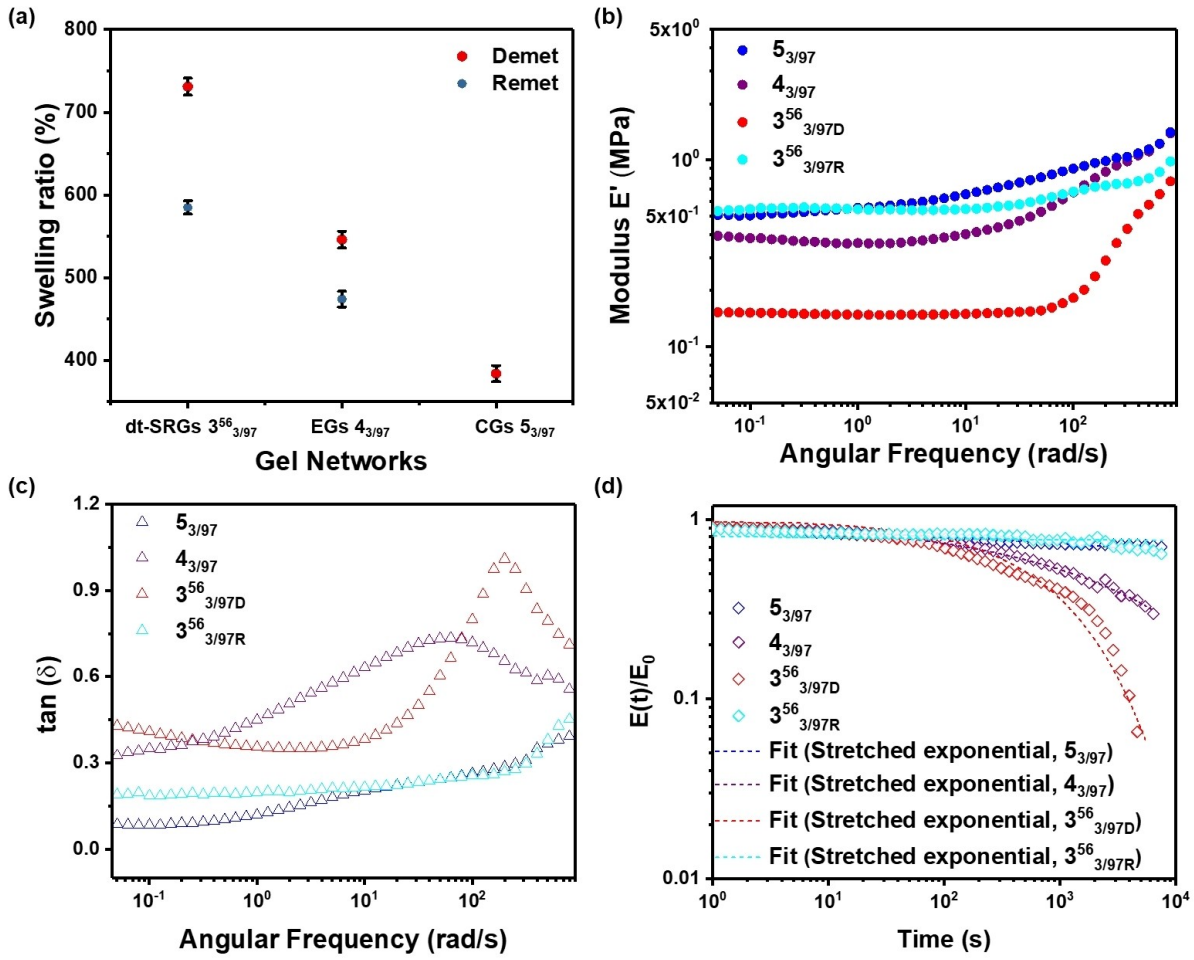

Figure 5. Effect of the ring crosslinking moieties on swelling behaviors and mechanical properties of the gels. (a) Swelling ratios of demetalated (red) and remetalated (purple) dt-SRG $\mathbf{3}^{\mathbf{56}}_{3/97}$, EG $\mathbf{4}_{3/97}$, and CG $\mathbf{5}_{3/97}$ in propylene carbonate (PC). (b) Storage moduli *E'* and (c) loss factor *tan δ* of demetalated (red) and remetalated (cyan) dt-SRG $\mathbf{3}^{\mathbf{56}}_{3/97}$, EG $\mathbf{4}_{3/97}$ (purple), and CG $\mathbf{5}_{3/97}$ (blue) fully swollen in PC. (d) Stress relaxation (strain 4%) curves (symbols) and fitted lines using the stretched exponential model (dashed lines) for demetalated (red) and remetalated (cyan) dt-SRG $\mathbf{3}^{\mathbf{56}}_{3/97}$, EG $\mathbf{4}_{3/97}$ (purple), and CG $\mathbf{5}_{3/97}$ (blue) fully swollen in PC.

dt-SRGs ($\mathbf{3}^{\mathbf{46}}_{3/97}$, $\mathbf{3}^{\mathbf{56}}_{3/97}$, and $\mathbf{3}^{\mathbf{68}}_{3/97}$) exhibited comparable gel fractions (~86 wt %) and high ring contents (>97 % of the macrocycle added to the reaction, Figure S28). Similar to $\mathbf{3}^{\mathbf{56}}_{3/97D}$, the demetalated dt-SRGs $\mathbf{3}^{\mathbf{46}}_{3/97}$ and $\mathbf{3}^{\mathbf{68}}_{3/97}$ also retained their ring components without any dethreading even after 10 days of exposure to chloroform at 50 °C (Figure S29).

To explore the impact of ring size on the gel network, the swelling ratio of three dt-SRGs ($\mathbf{3}^{\mathbf{46}}_{3/97}$, $\mathbf{3}^{\mathbf{56}}_{3/97}$, and $\mathbf{3}^{\mathbf{68}}_{3/97}$) was measured when they were fully swollen in PC (Figures 6a and S30). The swelling ratio of the demetalated dt-SRGs increases with ring size: $\mathbf{3}^{\mathbf{46}}_{3/97D}$ (610 %), $\mathbf{3}^{\mathbf{56}}_{3/97D}$ (720 %), and $\mathbf{3}^{\mathbf{68}}_{3/97D}$ (1260 %). Upon remetalation, the swelling ratio decreases in all dt-SRGs: $\mathbf{3}^{\mathbf{46}}_{3/97R}$ (520 %), $\mathbf{3}^{\mathbf{56}}_{3/97R}$ (580 %), and $\mathbf{3}^{\mathbf{68}}_{3/97R}$ (810 %). Interestingly, a smaller difference in the swelling ratio between demetalated and remetalated states is observed in dt-SRGs with the smaller ring, $\mathbf{3}^{\mathbf{46}}_{3/97D}$. Such differences in swelling behavior could be attributed to the slidable range of the dt-SR crosslinks,[43,44] which will depend on the ring size. It is certainly important to note that the three remetalated dt-SRGs do exhibit different degrees of swelling, with $\mathbf{3}^{\mathbf{68}}_{3/97R}$ showing greater swelling (ca. 800 %) relative to $\mathbf{3}^{\mathbf{46}}_{3/97R}$ and $\mathbf{3}^{\mathbf{56}}_{3/97R}$ (<600 %). This may, at least in part, be a result of the distinct chemical structures of the macrocycles involved. The $\mathbf{2}^{\mathbf{68}}$ has flexible ethylene glycol spacer units, while the $\mathbf{2}^{\mathbf{46}}$ and $\mathbf{2}^{\mathbf{56}}$ have rigid spacer units (*m*-xylene or *m*-naphthalene). The synergistic effect of the larger ring sizes and the flexibility of spacer units in the $\mathbf{2}^{\mathbf{68}}$ may contribute to additional swelling in $\mathbf{3}^{\mathbf{68}}_{3/97R}$.

The viscoelastic properties of the three demetalated dt-SRGs ($\mathbf{3}^{\mathbf{46}}_{3/97D}$, $\mathbf{3}^{\mathbf{56}}_{3/97D}$, and $\mathbf{3}^{\mathbf{68}}_{3/97D}$) were then examined. The extent of swelling directly influences the mesh size; therefore, the mechanical properties of gels would be expected to be closely related to their swelling behavior, given that these gels have comparable components and gel fractions. As discussed above, the swelling capacity of the dt-SRGs increases from $\mathbf{3}^{\mathbf{46}}_{3/97}$ to $\mathbf{3}^{\mathbf{68}}_{3/97}$, presumably on account of

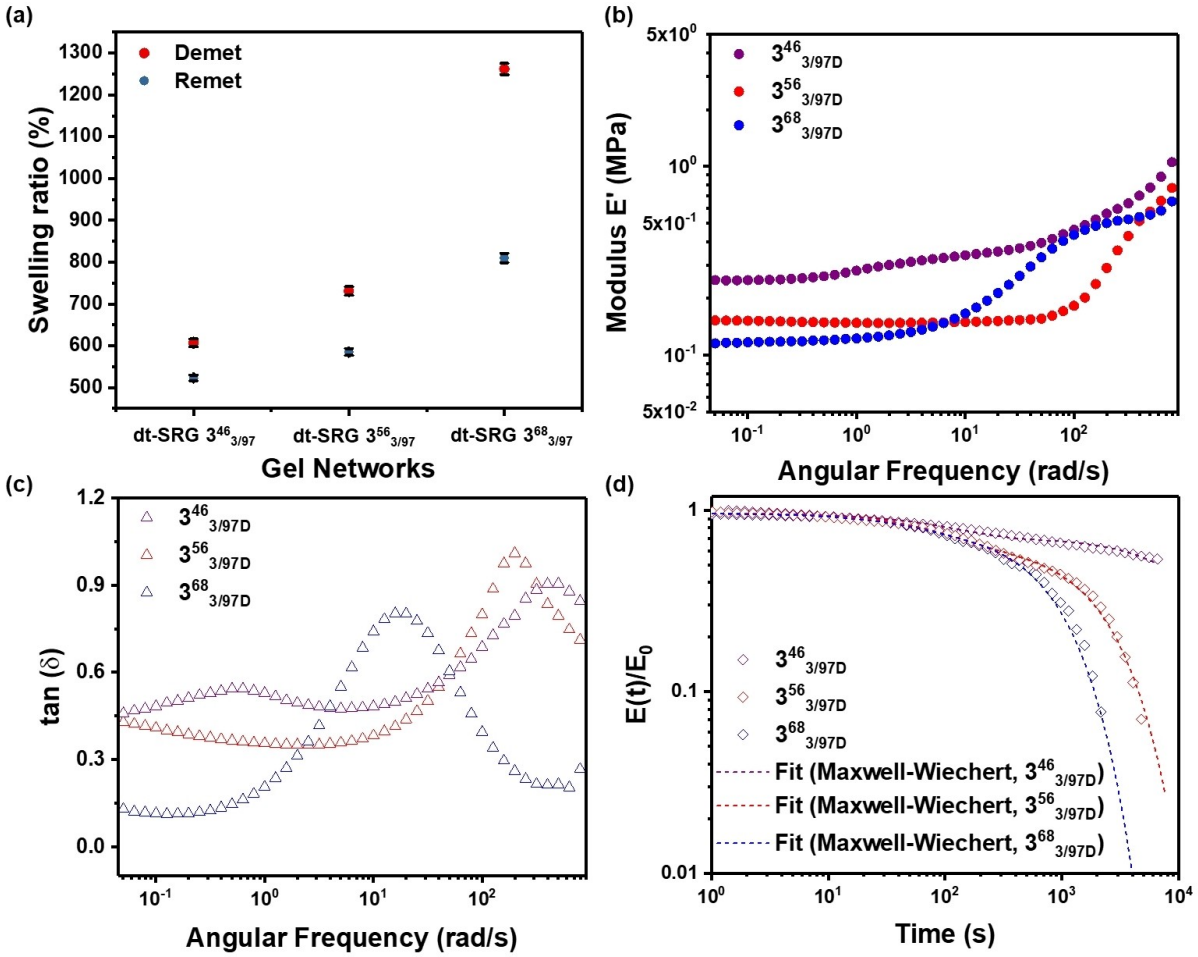

Figure 6. Effect of ring size on swelling behaviors and mechanical properties in three demetalated dt-SRGs. (a) Swelling ratios of demetalated (red) and remetalated (purple) dt-SRGs $\mathbf{3}^{\mathbf{46}}{}_{\mathbf{3/97}}$, $\mathbf{3}^{\mathbf{56}}{}_{\mathbf{3/97}}$, and $\mathbf{3}^{\mathbf{68}}{}_{\mathbf{3/97}}$ when exposed to propylene carbonate (PC). (b) Storage moduli E' and (c) loss factor *tan* δ of three demetalated dt-SRGs $\mathbf{3}^{\mathbf{46}}{}_{\mathbf{3/97D}}$ (purple), $\mathbf{3}^{\mathbf{56}}{}_{\mathbf{3/97D}}$ (red), $\mathbf{3}^{\mathbf{68}}{}_{\mathbf{3/97D}}$ (blue) fully swollen in PC. (d) Stress relaxation (strain 4%) measurements (symbols) and fitted lines using the Maxwell-Wiechert model (dashed lines) for three demetalated dt-SRGs $\mathbf{3}^{\mathbf{46}}{}_{\mathbf{3/97D}}$ (purple), $\mathbf{3}^{\mathbf{56}}{}_{\mathbf{3/97D}}$ (red), $\mathbf{3}^{\mathbf{68}}{}_{\mathbf{3/97D}}$ (blue) fully swollen in PC.

their enhanced slidable range of the bigger rings that results in a larger mesh size of the gel. To discern the effect of mesh size on the mechanical property, the moduli of the demetalated dt-SRGs $\mathbf{3}^{\mathbf{46}}{}_{\mathbf{3/97D}}$, $\mathbf{3}^{\mathbf{56}}{}_{\mathbf{3/97D}}$, and $\mathbf{3}^{\mathbf{68}}{}_{\mathbf{3/97D}}$ were compared in Figures 6b and S31. Their plateau storage modulus at angular frequency $\omega < 1$ rad/s decreases as the ring size increases: $E'_{\text{plateau}} = 250$ kPa for $\mathbf{3}^{\mathbf{46}}{}_{\mathbf{3/97D}}$, $E'_{\text{plateau}} = 150$ kPa for $\mathbf{3}^{\mathbf{56}}{}_{\mathbf{3/97D}}$, and $E'_{\text{plateau}} = 120$ kPa for $\mathbf{3}^{\mathbf{68}}{}_{\mathbf{3/97D}}$, a trend that is in good agreement with the observed swelling behavior. The gel geometries can be further discerned by estimating the mesh size from the plateau modulus. Based on a scaling relation, $E'_{\text{plateau}} \sim k_B T/\xi^3$ (where k_B is Boltzmann constant and T is temperature) between the bulk modulus E'_{plateau} and the mesh size (ξ), the unit volume and the mesh size ratio are estimated to be $(\xi_{3^{68}{}_{3/97D}}/\xi_{3^{46}{}_{3/97D}})^3$ ~2.1 and $(\xi_{3^{68}{}_{3/97D}}/\xi_{3^{46}{}_{3/97D}})$ ~1.3, respectively. The estimated unit volume ratio is consistent with the observed increase in swelling ratio $\Delta V_{3^{68}{}_{3/97D}}/\Delta V_{3^{46}{}_{3/97D}} = 1260/610 \sim 2.1$. Additionally, in the frequency range studied, dt-SRG $\mathbf{3}^{\mathbf{68}}{}_{\mathbf{3/97D}}$ exhibits a clear second plateau storage modulus regime at an angular frequency $\omega > 100$ rad/s. The presence of two plateau regimes could be attributed to the sliding transition of the rings.[45,49,50] The higher-frequency plateau regime could be assigned to the rubbery state, where there is little movement of the rings at these timescales. The lower-frequency plateau regime would then indicate a sliding state, where the timescale is such that the threaded polymer chains and rings are able to slide relative to each other. It would be expected that the sliding dynamics of polymer chains through rings would lead to a state with modulus lower than the rubbery plateau.[45,49,50] Furthermore, as depicted in Figure 6c, the three dt-SRGs ($\mathbf{3}^{\mathbf{46}}{}_{\mathbf{3/97D}}$, $\mathbf{3}^{\mathbf{56}}{}_{\mathbf{3/97D}}$, and $\mathbf{3}^{\mathbf{68}}{}_{\mathbf{3/97D}}$) exhibit a *tan* δ peak, which is presumed to be related to a sliding transition, at different frequencies, with a lower peak frequency for the dt-SRG with larger rings. This observation could be ascribed to variations in the characteristic length scale, specifically the mesh size ξ. In $\mathbf{3}^{\mathbf{68}}{}_{\mathbf{3/97D}}$ with a larger mesh size, a larger ring ($\mathbf{2}^{\mathbf{68}}$) can slide over a longer range. Thus, the sliding

relaxation occurs on a longer timescale, resulting in the *tan* δ peak at a lower frequency. In contrast, in $\mathbf{3^{46}_{3/97D}}$ with a smaller mesh size, the ring ($\mathbf{2^{46}}$) presumably slides within a more confined range, leading to the sliding relaxations on a shorter timescale. The difference in the slidable range of rings results in the shift of the *tan* δ peak frequency.

To further probe the effect of ring size on the ring mobility in these gels, macroscopic stress relaxation experiments were conducted, where a step strain ($\gamma = 4\,\%$) was applied to the dt-SRGs and the relaxation modulus E(t) was monitored over time (Figure S32). As shown in Figure 6d, all three dt-SRGs ($\mathbf{3^{46}_{3/97D}}$, $\mathbf{3^{56}_{3/97D}}$, and $\mathbf{3^{68}_{3/97D}}$) exhibit very different stress relaxation behavior depending on the mobility of the dt-SR crosslinks. As with the $\mathbf{3^{56}_{3/97D}}$ relaxation data described above, the Maxwell-Wiechert model with $n = 2$ could be utilized to fit the $\mathbf{3^{46}_{3/97D}}$ and $\mathbf{3^{68}_{3/97D}}$ dt-SRGs data and calculate their relaxation times. The dt-SRG $\mathbf{3^{68}_{3/97D}}$ with larger rings exhibits much faster relaxation at both the early-stage ($\tau_1 = 45$ s) and the late-stage ($\tau_2 = 900$ s), compared to the two relaxation times of $\mathbf{3^{56}_{3/97D}}$ ($\tau_1 = 95$ s and $\tau_2 = 2400$ s) discussed above. Especially noteworthy is the faster τ_1, presumably resulting from the sliding of backbone polymer strands through the ring, highlighting the higher mobility of $\mathbf{2^{68}}$ in the network, despite it being slightly larger in size (Figures S33–S35). In contrast, dt-SRG $\mathbf{3^{46}_{3/97D}}$ with the smallest rings exhibits the slowest stress relaxation ($\tau_1 = 125$ s and $\tau_2 = 22000$ s).

Conclusion

In conclusion, this study presents an approach to accessing dt-SRGs by introducing doubly threaded P3R crosslinkers that are self-assembled via metal-templating. Through photo-initiated copolymerization of these P3R crosslinkers with PEG-acrylate monomers, three dt-SRGs with varying size of the ring crosslinking moieties are successfully fabricated, and the physicochemical and mechanical properties of dt-SRGs are characterized and compared to those of corresponding entangled and covalent gels networks (EG and CG). The presence of the ring crosslinking moieties in dt-SRGs facilitates enhanced swelling and imparts unusual mechanical properties, as evidenced by their lower plateau storage modulus, distinct loss factor peak, and faster macroscopic stress relaxation. Additionally, the mechanical properties of dt-SRGs can be tuned by "locking" ring mobility through remetalation, demonstrating the effect of mobility of slide-ring crosslinks. Furthermore, the impact of ring sizes on dt-SRGs is explored. dt-SRG with larger rings exhibits a greater swelling degree, possibly due to enhanced slidable ranges and higher ring mobility, demonstrating softer mechanical properties and faster macroscopic stress relaxation behavior compared to those with smaller rings. This suggests that the ring mobility can be tailored by adjusting the ring size, offering a versatile platform for designing gel networks with desired properties. Overall, this research not only presents a new design strategy for dt-SRGs but also provides fundamental insights into the role of ring mobility in mechanically interlocked polymer architectures.

Supporting Information

Synthesis and characterization of monomers, supramolecular crosslinkers, and gels are detailed in the Supporting Information. The authors have cited additional references within the Supporting Information.

Acknowledgements

This work was funded by National Science Foundation (NSF) grant number CHE-2304633. This work made use of the shared facilities at the University of Chicago Materials Research Science and Engineering Center (MRSEC), supported by National Science Foundation (NSF) under award number DMR-2011854. We would like to thank the University of Chicago Chemistry NMR Facility and the facility manager Dr Josh Kurutz for helpful discussion on DOSY and ^{1}H T1 NMR analysis. Some parts of this work were carried out at the Soft Matter Characterization Facility (SMCF) of the University of Chicago. We would also like to thank the director of the SMCF, Dr. Philip Griffin, for his assistance with mechanical properties measurement.

Conflict of Interest

The authors declare no conflict of interest.

Data Availability Statement

The data that support the findings of this study are available from the corresponding author upon reasonable request.

Keywords: Mechanically interlocked polymers · Slide-ring networks · [3]rotaxane · Metal-coordination · Gel

[1] C. J. Bruns, J. F. Stoddart, *The Nature of the Mechanical Bond: From Molecules to Machines*, Wiley, Hoboken **2016**.
[2] J. F. Stoddart, *Chem. Soc. Rev.* **2009**, *38*, 1802–1820.
[3] J. F. Stoddart, *Angew. Chem. Int. Ed.* **2017**, *56*, 11094–11125.
[4] J. P. Sauvage, *Angew. Chem. Int. Ed.* **2017**, *56*, 11080–11093.
[5] S. J. Cantrill, S. J. Rowan, J. F. Stoddart, *Org. Lett.* **1999**, *1*, 1363–1366.
[6] J. J. Danon, D. A. Leigh, P. R. McGonigal, J. W. Ward, J. Wu, *J. Am. Chem. Soc.* **2016**, *138*, 12643–12647.
[7] I. T. Harrison, S. Harrison, *J. Am. Chem. Soc.* **1967**, *89*, 5723–5724.
[8] P. R. McGonigal, *Supramol. Chem.* **2018**, *30*, 782–794.
[9] H.-Y. Zhou, Q.-S. Zong, Y. Han, C.-F. Chen, *Chem. Commun.* **2020**, *56*, 9916–9936.
[10] S. J. Rowan, S. J. Cantrill, J. F. Stoddart, *Org. Lett.* **1999**, *1*, 129–132.
[11] J. A. Wisner, P. D. Beer, M. G. Drew, M. R. Sambrook, *J. Am. Chem. Soc.* **2002**, *124*, 12469–12476.
[12] C. Wu, P. R. Lecavalier, Y. X. Shen, H. W. Gibson, *Chem. Mater.* **1991**, *3*, 569–572.
[13] G. Gil-Ramirez, D. A. Leigh, A. J. Stephens, *Angew. Chem. Int. Ed.* **2015**, *54*, 6110–6150.

[14] R. S. Forgan, J. J. Gassensmith, D. B. Cordes, M. M. Boyle, K. J. Hartlieb, D. C. Friedman, A. M. Slawin, J. F. Stoddart, *J. Am. Chem. Soc.* **2012**, *134*, 17007–17010.
[15] C. P. Collier, G. Mattersteig, E. W. Wong, Y. Luo, K. Beverly, J. Sampaio, F. M. Raymo, J. F. Stoddart, J. R. Heath, *Science* **2000**, *289*, 1172–1175.
[16] F. B. Cougnon, N. A. Jenkins, G. D. Pantoş, J. K. Sanders, *Angew. Chem. Int. Ed.* **2012**, *51*, 1443–1447.
[17] S. D. Fielden, D. A. Leigh, S. L. Woltering, *Angew. Chem. Int. Ed.* **2017**, *56*, 11166–11194.
[18] K. S. Chichak, S. J. Cantrill, A. R. Pease, S.-H. Chiu, G. W. Cave, J. L. Atwood, J. F. Stoddart, *Science* **2004**, *304*, 1308–1312.
[19] J. J. Danon, A. Krüger, D. A. Leigh, J.-F. Lemonnier, A. J. Stephens, I. J. Vitorica-Yrezabal, S. L. Woltering, *Science* **2017**, *355*, 159–162.
[20] J.-F. Ayme, J. E. Beves, C. J. Campbell, D. A. Leigh, *Chem. Soc. Rev.* **2013**, *42*, 1700–1712.
[21] L. F. Hart, J. E. Hertzog, P. M. Rauscher, B. W. Rawe, M. M. Tranquilli, S. J. Rowan, *Nat. Rev. Mater.* **2021**, *6*, 508–530.
[22] L. Chen, X. Sheng, G. Li, F. Huang, *Chem. Soc. Rev.* **2022**, *51*, 7046–7065.
[23] S. J. Rao, K. Nakazono, X. Liang, K. Nakajima, T. Takata, *Chem. Commun.* **2019**, *55*, 5231–5234.
[24] R. Tao, Q. Zhang, S. Rao, X. Zheng, M. Li, D. Qu, *Sci. China Chem.* **2019**, *62*, 245–250.
[25] C. Y. Shi, Q. Zhang, C. Y. Yu, S. J. Rao, S. Yang, H. Tian, D. H. Qu, *Adv. Mater.* **2020**, *32*, 2000345.
[26] M. A. Olson, A. B. Braunschweig, L. Fang, T. Ikeda, R. Klajn, A. Trabolsi, P. J. Wesson, D. Benítez, C. A. Mirkin, B. A. Grzybowski, J. F. Stoddart, *Angew. Chem. Int. Ed.* **2009**, *121*, 1824–1829.
[27] M. M. Tranquilli, Q. Wu, S. J. Rowan, *Chem. Sci.* **2021**, *12*, 8722–8730.
[28] M. M. Tranquilli, B. W. Rawe, G. Liu, S. J. Rowan, *Chem. Sci.* **2023**, *14*, 2596–2605.
[29] Q. Wu, P. M. Rauscher, X. Lang, R. J. Wojtecki, J. J. De Pablo, M. J. Hore, S. J. Rowan, *Science* **2017**, *358*, 1434–1439.
[30] G. Liu, P. M. Rauscher, B. W. Rawe, M. M. Tranquilli, S. J. Rowan, *Chem. Soc. Rev.* **2022**, *51*, 4928–4948.
[31] Y. Okumura, K. Ito, *Adv. Mater.* **2001**, *13*, 485–487.
[32] E. Lee, J. Heo, K. Kim, *Angew. Chem. Int. Ed.* **2000**, *112*, 2811–2813.
[33] J. Araki, C. Zhao, K. Ito, *Macromolecules* **2005**, *38*, 7524–7527.
[34] P. G. Clark, M. W. Day, R. H. Grubbs, *J. Am. Chem. Soc.* **2009**, *131*, 13631–13633.
[35] L. Fang, M. Hmadeh, J. Wu, M. A. Olson, J. M. Spruell, A. Trabolsi, Y.-W. Yang, M. Elhabiri, A.-M. Albrecht-Gary, J. F. Stoddart, *J. Am. Chem. Soc.* **2009**, *131*, 7126–7134.
[36] K. Iwaso, Y. Takashima, A. Harada, *Nat. Chem.* **2016**, *8*, 625–632.
[37] G. Fleury, G. Schlatter, C. Brochon, C. Travelet, A. Lapp, P. Lindner, G. Hadziioannou, *Macromolecules* **2007**, *40*, 535–543.
[38] C. Liu, H. Kadono, K. Mayumi, K. Kato, H. Yokoyama, K. Ito, *ACS Macro Lett.* **2017**, *6*, 1409–1413.
[39] W. Wang, H. Xing, *Polym. Chem.* **2018**, *9*, 2087–2091.
[40] H. Xing, Z. Li, Z. L. Wu, F. Huang, *Macromol. Rapid Commun.* **2018**, *39*, 1700361.
[41] M. A. Nosiglia, N. D. Colley, M. K. Danielson, M. S. Palmquist, A. O. Delawder, S. L. Tran, G. H. Harlan, J. C. Barnes, *J. Am. Chem. Soc.* **2022**, *144*, 9990–9996.
[42] K. Ito, *Polym. J.* **2007**, *39*, 489–499.
[43] L. Jiang, C. Liu, K. Mayumi, K. Kato, H. Yokoyama, K. Ito, *Chem. Mater.* **2018**, *30*, 5013–5019.
[44] A. Konda, K. Mayumi, K. Urayama, T. Takigawa, K. Ito, *Macromolecules* **2012**, *45*, 6733–6740.
[45] K. Ito, *Polym. J.* **2012**, *44*, 38–41.
[46] K. Mayumi, M. Tezuka, A. Bando, K. Ito, *Soft Matter* **2012**, *8*, 8179–8183.
[47] H. Gotoh, C. Liu, A. B. Imran, M. Hara, T. Seki, K. Mayumi, K. Ito, Y. Takeoka, *Sci. Adv.* **2018**, *4*, eaat7629.
[48] Y. Yasuda, T. Masumoto, K. Mayumi, M. Toda, H. Yokoyama, H. Morita, K. Ito, *ACS Macro Lett.* **2020**, *9*, 1280–1285.
[49] K. Kato, K. Ito, *Soft Matter* **2011**, *7*, 8737–8740.
[50] K. Kato, T. Yasuda, K. Ito, *Macromolecules* **2013**, *46*, 310–316.
[51] J. Sawada, D. Aoki, M. Kuzume, K. Nakazono, H. Otsuka, T. Takata, *Polym. Chem.* **2017**, *8*, 1878–1881.
[52] J. Sawada, D. Aoki, S. Uchida, H. Otsuka, T. Takata, *ACS Macro Lett.* **2015**, *4*, 598–601.
[53] K. Yamamoto, R. Nameki, H. Sogawa, T. Takata, *Angew. Chem. Int. Ed.* **2020**, *59*, 18023–18028.
[54] M. Ogawa, H. Sogawa, Y. Koyama, T. Takata, *Polym. J.* **2015**, *47*, 580–584.
[55] J. Sawada, D. Aoki, H. Otsuka, T. Takata, *Angew. Chem. Int. Ed.* **2019**, *131*, 2791–2794.
[56] Y. Akae, J. Sawada, K. Nakajima, T. Takata, *Angew. Chem. Int. Ed.* **2023**, *62*, e202303341.
[57] L. F. Hart, W. R. Lenart, J. E. Hertzog, J. Oh, W. R. Turner, J. M. Dennis, S. J. Rowan, *J. Am. Chem. Soc.* **2023**, *145*, 12315–12323.
[58] J. E. Hertzog, V. J. Maddi, L. F. Hart, B. W. Rawe, P. M. Rauscher, K. M. Herbert, E. P. Bruckner, J. J. de Pablo, S. J. Rowan, *Chem. Sci.* **2022**, *13*, 5333–5344.
[59] J. E. Hertzog, G. Liu, B. W. Rawe, V. J. Maddi, L. F. Hart, J. Oh, N. D. Dolinski, S. J. Rowan, *Org. Biomol. Chem.* **2023**, *21*, 6969–6978.
[60] M. Tang, D. Zheng, J. Samanta, E. H. Tsai, H. Qiu, J. A. Read, C. Ke, *Chem* **2023**, *9*, 3515–3531.
[61] J. Lou, S. Friedowitz, K. Will, J. Qin, Y. Xia, *Adv. Mater.* **2021**, *33*, 2104460.
[62] Q. Li, D. G. Barrett, P. B. Messersmith, N. Holten-Andersen, *ACS Nano* **2016**, *10*, 1317–1324.
[63] F. Meng, R. H. Pritchard, E. M. Terentjev, *Macromolecules* **2016**, *49*, 2843–2852.
[64] M. Guerre, C. Taplan, J. M. Winne, F. E. Du Prez, *Chem. Sci.* **2020**, *11*, 4855–4870.

Manuscript received: June 13, 2024
Accepted manuscript online: August 19, 2024
Version of record online: September 10, 2024